

Estimating black carbon aging time-scales with a particle-resolved aerosol model

Nicole Riemer ^{a,*}, Matthew West ^b, Rahul Zaveri ^c,
Richard Easter ^c

^a*Department of Atmospheric Science, University of Illinois at Urbana-Champaign,
Urbana, Illinois, USA*

^b*Department of Mechanical Science and Engineering, University of Illinois at
Urbana-Champaign, Urbana, Illinois, USA*

^c*Atmospheric Science and Global Change Division, Pacific Northwest National
Laboratory, Richland, Washington, USA*

Abstract

Understanding the aging process of aerosol particles is important for assessing their chemical reactivity, cloud condensation nuclei activity, radiative properties and health impacts. In this study we investigate the aging of black carbon containing particles in an idealized urban plume using a new approach, the particle-resolved aerosol model PartMC-MOSAIC. We present a method to estimate aging time-scales using an aging criterion based on cloud condensation nuclei activation. The results show a separation into a daytime regime where condensation dominates and a nighttime regime where coagulation dominates. For the chosen urban plume scenario, depending on the supersaturation threshold, the values for the aging time-scales vary between 0.06 hours and 10 hours during the day, and between 6 hours and 20 hours during the night.

Key words: black carbon, aerosol aging, mixing state, CCN

1 Introduction

2 Black carbon containing particles, or “soot” particles, are ubiquitous in the
3 atmosphere and their role for regional and global climate has been widely rec-
4 ognized (IPCC, 2007). Since black carbon absorbs light (Horvath and Trier,

* Corresponding author

Email address: nriemer@illinois.edu (Nicole Riemer).

5 1993), it contributes to the aerosol radiative forcing, potentially partially off-
6 setting the cooling effect of scattering aerosol particles such as sulfates (Menon
7 et al., 2002).

8 Black carbon containing particles originate from the incomplete combustion of
9 carbon containing material, hence emissions from traffic are an important con-
10 tributor (Bond et al., 2004). Other important sources for black carbon include
11 biomass burning and the combustion of coal by industrial processes. In this
12 paper we focus on black carbon from traffic emissions. Measurements of vehi-
13 cle emissions from gasoline and diesel cars show that the emitted particles are
14 a complex mixture of many chemical species with the main constituents being
15 black carbon and organic carbon (Medalia and Rivin, 1982; Toner et al., 2006).
16 Trace concentrations of ionic and metallic species are also present (Kleeman
17 et al., 2000). The exact composition depends on several factors, including the
18 fuel type, the operating conditions and the condition of the individual vehicles.

19 During their transport in the atmosphere, the composition of these particle
20 emissions are further modified. Coagulation, condensation and photochemistry
21 are contributing processes, collectively known as aging (Weingartner et al.,
22 1997). During this aging process the composition of the individual particles
23 or, in other words, their mixing states change (Furutani et al., 2008). This
24 impacts the particles’ physico-chemical properties including their chemical
25 reactivity, radiative properties and health impacts. In particular, the aging
26 process can change the particles’ hygroscopicity from initially hydrophobic to
27 more hydrophilic, and hence change their ability to become cloud condensa-
28 tion nuclei (McFiggans et al., 2006; McMurry and Stolzenburg, 1989; Moffet
29 et al., 2008; Cubison et al., 2008).

30 This is important as models and observations suggest that wet deposition
31 represents 70–85% of the tropospheric sink for carbonaceous aerosol mass
32 (Pöschl, 2005). As a consequence, to assess the budget and impact of black
33 carbon, models need to capture the aging process adequately. Many global
34 models have simulated both (fresh) hydrophobic black carbon and (aged) hy-
35 drophilic black carbon, which can be considered a minimal representation of
36 the black carbon mixing state (Cooke et al., 1999; Lohmann et al., 1999; Koch,
37 2001; Croft et al., 2005). In such a framework only the hydrophilic black car-
38 bon is subject to in-cloud scavenging. The conversion from hydrophobic to
39 hydrophilic is frequently modeled as a first-order system with the single pa-
40 rameter of aging rate or its inverse, the aging time-scale τ which represents the
41 time-scale on which a population of black carbon containing particles transfers
42 from the “fresh” category to the “aged” category.

43 While conceptually simple, the actual value of the aging time-scale τ is not
44 well constrained. Koch (2001) and Croft et al. (2005) compared different ag-
45 ing parameterizations in global models and concluded that the model results

46 critically depended on the respective formulation. Riemer et al. (2004) used
47 mesoscale simulations to determine τ . They derived the aging time-scale for
48 black carbon particles as a function of height and time of the day, which sug-
49 gested that assuming a single parameter for the black carbon aging time-scale
50 is an oversimplification that will incorrectly estimate the black carbon burden.
51 However, even though this treatment allowed more detailed insight into the
52 aging process, it was still based on ad hoc aging rules inherent to the modal
53 model framework that was used (Riemer et al., 2003).

54 Recently, Riemer et al. (2009) developed a particle-resolved aerosol model,
55 PartMC-MOSAIC, which explicitly resolves the composition of individual par-
56 ticles in a given population of different types of aerosol particles, so that no
57 ad hoc aging criteria needs to be invoked. They applied PartMC-MOSAIC
58 in a Lagrangian box-model framework to an idealized urban plume scenario
59 to study the evolution of urban aerosols due to coagulation and condensation
60 over the course of 24 hours.

61 In this study, we build upon Riemer et al. (2009) and present a method for es-
62 timating aging time-scales of black carbon containing particles using PartMC-
63 MOSAIC, based on the idealized urban plume scenario. We take the particle
64 population simulated in Riemer et al. (2009) and use a CCN-based aging cri-
65 teria to determine whether each individual particle is fresh or aged at every
66 timestep, and how many particles transfer between the fresh and aged cate-
67 gories during each timestep. By fitting these results to a first-order bulk model
68 of aerosol aging we are able to determine the aging timescale without mak-
69 ing any a priori assumptions about the aging process. To our knowledge it
70 is the first time that a method is presented for explicitly calculating aging
71 time-scales.

72 Section 2 introduces the model system. In Section 3 we describe the idealized
73 plume scenario that served as a basis for the time-scale estimation. Section 4
74 presents our method for deriving time-scales from our model and Section 5
75 shows the results. We summarize our findings in Section 6.

76 **2 Model description**

77 PartMC-MOSAIC is a particle-resolved model that simulates the evolution of
78 individual aerosol particles and trace gases in a single parcel (or volume) of
79 air moving along a specified trajectory. For each particle the mass of each con-
80 stituent species is tracked, but the particle position in space is not simulated,
81 making this a zero-dimensional or box model. In addition to coagulation and
82 aerosol- and gas-phase chemistry, the model includes prescribed emissions of
83 aerosols and gases, and mixing of the parcel with background air. The simu-

84 lation results shown here use around 100,000 particles in a volume of around
85 16 cm^3 (the precise values vary over the course of the simulation). We regard
86 this volume as being representative of a much larger air parcel. The model
87 accurately predicts both number and mass size distributions and is therefore
88 suited for applications where either quantity is required. Details of PartMC-
89 MOSAIC and the urban plume scenario are described in Riemer et al. (2009).
90 Here we give a brief summary.

91 The simulation of the aerosol state proceeds by two mechanisms. First, the
92 composition of each particle can change as species condense from the gas phase
93 and evaporate to it. Second, the aerosol population can have particles added
94 and removed, either by coagulation events between particles, by emissions,
95 or by dilution. While condensation/evaporation is handled deterministically,
96 emission, dilution and coagulation are treated with a stochastic approach.

97 Coagulation between aerosol particles is simulated in PartMC by generating
98 a realization of a Poisson process with a Brownian coagulation kernel. For
99 the large number of particles used here it is necessary to employ an efficient
100 approximate simulation method. We developed a binned sampling method
101 to efficiently sample from the highly multi-scale coagulation kernel (in our
102 case the Brownian kernel) in the presence of a very non-uniform particle size
103 distribution, which is described in detail in Riemer et al. (2009).

104 Particle emissions and dilution with background air are also implemented
105 in a stochastic manner. Because we are using a finite number of particles to
106 approximate the current aerosol population, we need to add a finite number of
107 emitted particles to the volume at each timestep. Over time these finite particle
108 samplings should approximate the continuum emission distribution, so the
109 samplings at each timestep must be different. As for coagulation, we assume
110 that emissions are memoryless, so that emission of each particle is uncorrelated
111 with emission of any other particle. Under this assumption the appropriate
112 statistics are Poisson distributed, whereby the distribution of finite particles
113 is parametrized by the mean emission rate and distribution.

114 Lastly, we must also obtain a finite sampling of background particles that have
115 diluted into our computational volume during each timestep. In addition, some
116 of the particles in our current sample will dilute out of our volume and will
117 be lost, so this must be sampled as well. Again, we assume that dilution is
118 memoryless, so that dilution of each particle is uncorrelated with the dilution
119 of any other particle or itself at other times, and that once a particle dilutes
120 out it is lost.

121 We coupled the stochastic PartMC particle-resolved aerosol model to the de-
122 terministic MOSAIC gas- and aerosol-chemistry code (Zaveri et al., 2008)
123 in a time- or operator-splitting fashion (Press et al., 2007, Section 20.3.3).

124 MOSAIC treats all the globally important aerosol species including sulfate,
125 nitrate, chloride, carbonate, ammonium, sodium, calcium, primary organic
126 aerosol (POA), secondary organic aerosol (SOA), black carbon (BC), and in-
127 ert inorganic mass.

128 MOSAIC consists of four computationally efficient modules: 1) the gas-phase
129 photochemical mechanism CBM-Z (Zaveri and Peters, 1999); 2) the Multicom-
130 ponent Taylor Expansion Method (MTEM) for estimating activity coefficients
131 of electrolytes and ions in aqueous solutions (Zaveri et al., 2005b); 3) the Mul-
132 ticomponent Equilibrium Solver for Aerosols (MESA) for intra-particle solid-
133 liquid partitioning (Zaveri et al., 2005a); and 4) the Adaptive Step Time-split
134 Euler Method (ASTEM) for dynamic gas-particle partitioning over size- and
135 composition-resolved aerosol (Zaveri et al., 2008). The version of MOSAIC
136 implemented here also includes a treatment for SOA based on the SORGAM
137 scheme (Schell et al., 2001).

138 **3 Idealized urban plume scenario**

139 For our urban plume scenario, we tracked the evolution of gas phase species
140 and aerosol particles in a Lagrangian air parcel that initially contained back-
141 ground air and was advected over and beyond a large urban area, as described
142 in Riemer et al. (2009). The simulation started at 06:00 local standard time
143 (LST), and during the advection process, primary trace gases and aerosol par-
144 ticles from different sources were emitted into the air parcel for the duration
145 of 12 hours. After 18:00 LST, all emissions were switched off, and the evo-
146 lution of the air parcel was tracked for another 12 hours. The time series of
147 temperature, relative humidity and mixing height are shown in Figure 1.

148 Initial gas-phase and aerosol particle concentrations as well as gas phase and
149 particle emissions were the same as in Riemer et al. (2009). The gas phase
150 emissions varied throughout the emission time interval according to a typical
151 diurnal cycle found in polluted urban areas.

152 The initial particle distribution, which was identical to the background aerosol
153 distribution, was bimodal with Aitken and accumulation modes (Jaenicke,
154 1993). We assumed that it consisted of $(\text{NH}_4)_2\text{SO}_4$ and POA, as shown in Ta-
155 ble 1. We considered three different types of carbonaceous aerosol emissions:
156 1) meat cooking aerosol, 2) diesel vehicle emissions, and 3) gasoline vehicle
157 emissions. The parameters for the distributions of these three emission cate-
158 gories were based on Eldering and Cass (1996), Kittelson et al. (2006a), and
159 Kittelson et al. (2006b), respectively. For simplicity in this idealized study, the
160 particle emissions strength and their size distribution and composition were
161 kept constant with time during the time period of emission.

162 Furthermore, we assumed that every particle from a given source had the
 163 same composition, with the species listed in Table 1, since to date the mixing
 164 state of particle emissions is still not well quantified. In particular, we assume
 165 that the diesel and gasoline exhaust particles consist exclusively of POA and
 166 BC, which is very nearly the case (Andreae and Gelencsér, 2006; Medalia and
 167 Rivin, 1982; Kleeman et al., 2000).

168 Figure 2 shows time series of the bulk aerosol mass concentrations as they
 169 result from this urban plume scenario. We observed a pronounced production
 170 of ammonium nitrate, reaching nitrate mass concentration of up to $26 \mu\text{g m}^{-3}$
 171 and ammonium mass concentration of $10 \mu\text{g m}^{-3}$ in the late afternoon. Sulfate
 172 mass concentrations increased from $4.1 \mu\text{g m}^{-3}$ to $6.0 \mu\text{g m}^{-3}$ due to conden-
 173 sation of photochemically produced sulfuric acid. POA and BC were directly
 174 emitted (with a temporally constant rate) and accumulated to $11 \mu\text{g m}^{-3}$ and
 175 $4.3 \mu\text{g m}^{-3}$, respectively, until 18:00 LST when the emissions stopped. After
 176 18:00 LST the mass concentrations declined due to dilution, especially nitrate
 177 and BC for which the background mass concentration were zero.

178 3.1 Characterizing mixing state

To characterize the mixing state and to discuss the composition of a particle,
 we refer to the BC mass fractions as

$$w_{\text{BC,dry}} = \frac{\mu_{\text{BC}}}{\mu_{\text{dry}}} \quad (1)$$

179 where μ_{BC} is the mass of BC in a given particle and μ_{dry} is the total dry mass.

180 Based on this quantity, we then define a two-dimensional number concen-
 181 tration that is a function of both particle composition and diameter. The
 182 two-dimensional cumulative number distribution $N_{\text{BC,dry}}(w, D)$ is the number
 183 of particles per volume that have a diameter less than D and a BC mass
 184 fraction of less than w . The top panels in Figure 3 show the corresponding
 185 two-dimensional distributions, normalized with the respective total number
 186 concentrations, after 1 hour and after 24 hours of simulation time. Since even
 187 at the time of emission no particles were pure BC, particles were not present
 188 at $w_{\text{BC,dry}} = 100\%$. Fresh emissions from diesel vehicles ($w_{\text{BC,dry}} = 70\%$) and
 189 gasoline vehicles ($w_{\text{BC,dry}} = 20\%$) appear as horizontal lines since particles
 190 in one emission category were all emitted with the same composition. At
 191 $w_{\text{BC,dry}} = 0\%$ all the particles appear that do not contain any BC (i.e. back-
 192 ground particles and particles from meat cooking emissions that have not un-
 193 dergone coagulation with particles containing BC). After 1 hour (07:00 LST)
 194 a small number of particles between these three classes indicate the occur-
 195 rence of coagulation. Comparing this result to the result for the end of the

196 simulation, we note that at the end of the simulation particles with diameter
 197 below $D = 0.03 \mu\text{m}$ were heavily depleted due to coagulation. A continuum of
 198 mixing states formed between the extreme mixing states of $w_{\text{BC,dry}} = 0\%$ and
 199 $w_{\text{BC,dry}} = 70\%$.

200 3.2 Calculating CCN activity

201 Given that we track the composition evolution of each individual particle
 202 throughout the simulation, we can calculate the critical supersaturation S_c
 203 that the particle needs in order to activate. We use the concept of a dimen-
 204 sionless hygroscopicity parameter suggested by Ghan et al. (2001) or Petters
 205 and Kreidenweis (2007). In Petters and Kreidenweis (2007) this parameter is
 206 denoted by κ , and we adopt their notation for the remainder of the paper.
 207 This concept has the advantage that results from laboratory measurements
 208 can be used to quantify the hygroscopicity of complex compounds for which
 209 κ values cannot be calculated in a straightforward manner. The overall κ for
 210 a particle is the volume-weighted average of the κ values of the constituent
 211 species. This requires the assignment of individual κ values for each aerosol
 212 component in MOSAIC.

Petters and Kreidenweis (2007) compiled a table (Table 1 in their paper) with
 κ values for a variety of inorganic and organic species based on recent labora-
 tory measurements or on thermodynamic model calculations. For $(\text{NH}_4)_2\text{SO}_4$
 and NH_4NO_3 they report κ values of 0.61 and 0.67, based on calculations
 by Clegg et al. (1998) and measurements by Svenningsson et al. (2006), re-
 spectively. Based on this we assume $\kappa = 0.65$ for all salts formed from the
 $\text{NH}_4^+ - \text{SO}_4^{2-} - \text{NO}_3^-$ system. For all MOSAIC model species that represent SOA
 we assume $\kappa = 0.1$, based on measurements by Prenni et al. (2007). Following
 Petters et al. (2006) we assume $\kappa = 0.001$ for POA and $\kappa = 0$ for BC. The
 critical supersaturation S_c for a particle of diameter D and volume-weighted
 hygroscopicity parameter κ is then given by

$$S_c = \frac{C}{\sqrt{\kappa D^3}}, \quad (2)$$

where

$$C = \sqrt{\frac{4A^3}{27}} \quad \text{and} \quad A = \frac{4\sigma_w m_w}{R^* T \rho_w}, \quad (3)$$

213 with σ_w being the surface tension of water, m_w the molecular weight of water,
 214 R^* the universal gas constant, ρ_w the water density, and T the temperature.

215 Similarly to the use of $w_{\text{BC,dry}}$ above, we can use S_c to define a two-dimensional
 216 cumulative number distribution $N_S(D, S_c)$ in terms of size and critical super-
 217 saturation. The bottom panels in Figure 3 show examples of the corresponding

218 two-dimensional distributions after 1 hour (left) and after 24 hours (right) of
219 simulation. While freshly emitted diesel, gasoline and meat cooking particles
220 differ in their BC and POA mass fractions, they are very similar in their hy-
221 groscopicity with initial κ values close to zero. After 1 hour they are visible
222 as the dark band of high number concentrations at high S_c values. Separated
223 from this we see another dark band representing the most hygroscopic parti-
224 cles, consisting of wet background particles. They contain the largest fraction
225 of inorganic mass (ammonium, sulfate, and nitrate), hence their critical su-
226 persaturation is lowest at a given size compared to the other particle classes.

227 Directly slightly above the most hygroscopic band at 1 hour is a weaker band,
228 which represents the dry background particles. Because they are dry and the
229 vapor pressure of HNO_3 is still low, nitrate formation does not occur on these
230 particles. The coexistence of wet and dry particles can be explained by the
231 fact that the relative humidity falls below 85% at 06:42 LST, which is the deli-
232 quescence point of the inorganic mixture of ammonium, sulfate, and nitrate.
233 Particles that exist before that time contain water and take up nitrate. They
234 stay wet throughout the whole day as a result of the hysteresis of particle
235 deliquescence and crystallization. Particles that are emitted after 06:42 LST
236 do not contain water and take up nitrate only much later. Hence after 1 hour
237 of simulation, at a given size the fraction of highly hygroscopic inorganics is
238 higher for the wet particles, which results in a higher κ value and lower critical
239 supersaturation S_c .

240 The individual bands are not completely separated at 1 hour, but the regions
241 in between have started to fill out. The reason for this is the occurrence of
242 coagulation, which produces particles of intermediate composition and hence
243 corresponding intermediate S_c values. After 24 hours the population as a whole
244 has moved to lower critical supersaturations, and the distribution with respect
245 to S_c has become more continuous. Given a certain size, the critical supersat-
246 uration ranges over about one order of magnitude.

247 Figure 4 shows CCN properties as more traditional CCN spectra. This repre-
248 sentation is the one-dimensional projection of the bottom panels of Figure 3
249 onto the critical supersaturation axis, plotted as a cumulative distribution.
250 The change in CCN properties over the course of 24 hours is obvious. After
251 1 hour a supersaturation of $S = 1.5\%$ is necessary to activate 50% of the
252 particles by number. This required supersaturation decreases to $S = 0.1\%$
253 after 24 hours. In the following section we use the results of this urban plume
254 scenario as a basis for estimating the aging time-scales.

255 **4 First-order Models of Aging**

256 In this section we describe the first-order model of black carbon aging to which
 257 we fit the particle-resolved data simulated with PartMC-MOSAIC, in order
 258 to determine the aging time-scale. We emphasize that we do not actually
 259 simulate using the first-order models presented in this section. Such first-
 260 order systems are frequently used, however, to model the conversion from
 261 hydrophobic to hydrophilic black carbon with the single parameter of aging
 262 rate or its inverse, the aging time-scale τ (Croft et al., 2005). More specifically,
 263 the aging time-scale represents the time-scale on which particles that would
 264 initially not activate turn into particles that can be activated, given a certain
 265 chosen supersaturation threshold. Budget equations for the fresh and aged
 266 populations can be formulated in terms of either number or mass. A number
 267 based aging time-scale is relevant for aerosol indirect forcing as the cloud
 268 optical properties depend on the cloud droplet number distribution. On the
 269 other hand, a mass aging time-scale is relevant for in-cloud scavenging and wet
 270 removal of BC mass. In the following we will present results for both number-
 271 and mass-based aging time-scales.

272 At time t , the total number concentration $N_{\text{BC}}(t)$ of BC-particles is the sum
 273 of the number concentration of BC-containing fresh particles $N_{\text{f}}(t)$ and the
 274 number concentration of BC-containing aged particles $N_{\text{a}}(t)$. We define anal-
 275 ogously the total BC mass concentration $M_{\text{BC}}(t)$, the BC mass concentration
 276 in fresh BC-containing particles $M_{\text{f}}(t)$, and the BC mass concentration in aged
 277 BC-containing particles $M_{\text{a}}(t)$. The aged and fresh populations are separated
 278 by applying an aging criterion, in our case activation at a certain supersat-
 279 uration threshold S_{c} . Fresh particles are those with critical supersaturation
 280 above the threshold value, while aged particles have critical supersaturations
 281 below the threshold.

In the PartMC model we explicitly track a finite number of particles in a com-
 putational volume V . The number of fresh and aged BC-containing particles
 in the volume $V(t_k)$ at time t_k is denoted by $n_{\text{f}}(t_k)$ and $n_{\text{a}}(t_k)$, respectively.
 Similarly, $m_{\text{f}}(t_k)$ and $m_{\text{a}}(t_k)$ are respectively the total mass of BC in fresh and
 aged BC-containing particles in $V(t_k)$. The number and mass concentrations
 of fresh BC-containing particles in $V(t_k)$ are then given by

$$\begin{aligned}
 N_{\text{f}}(t_k) &= \frac{n_{\text{f}}(t_k)}{V(t_k)} & M_{\text{f}}(t_k) &= \frac{m_{\text{f}}(t_k)}{V(t_k)} \\
 N_{\text{a}}(t_k) &= \frac{n_{\text{a}}(t_k)}{V(t_k)} & M_{\text{a}}(t_k) &= \frac{m_{\text{a}}(t_k)}{V(t_k)}.
 \end{aligned}
 \tag{4}$$

282 The fresh and aged number and mass concentrations can change due to emis-
 283 sion and dilution, while condensation and coagulation can transfer number

284 and mass concentration from the fresh to the aged population and vice versa.
 285 Changes in number and mass concentrations also occur due to temperature
 286 and pressure changes. In our model we neglect at present the impact of hetero-
 287 geneous reactions on the surface of the particles, although studies have shown
 288 that these also contribute to the aging process (Rudich et al., 2007). The gain
 289 and loss terms for the fresh and aged BC-containing populations are given in
 290 Table 2.

291 To express changes in number and mass for coagulation we consider that all
 292 constituent particles are lost during a coagulation event and the product of
 293 coagulation is a gain of a new particle. Table 3 shows the overview of all
 294 possible combinations and the resulting terms for each of those combinations.
 295 For example, let us assume that there are four independent coagulation events
 296 within a single timestep: one event between two fresh BC-containing particles
 297 resulting in an aged particle, two events between fresh and aged BC-containing
 298 particles each resulting in an aged particle, and one event between a fresh
 299 BC-containing particle and a non-BC-containing particle resulting in a fresh
 300 particle. Then we have losses $\Delta n_{f \rightarrow a}^{\text{coag}}(t_{k-1}, t_k) = 5$ and $\Delta n_{a \rightarrow a}^{\text{coag}}(t_{k-1}, t_k) = 2$,
 301 and gains $\Delta n_f^{\text{coag}}(t_{k-1}, t_k) = 1$ and $\Delta n_a^{\text{coag}}(t_{k-1}, t_k) = 3$.

302 Note that for each particle pairing in Table 3 there can be two outcomes. For
 303 example, coagulation of a small fresh and large aged particle generally pro-
 304 duces an aged particle, while coagulation of large fresh and small aged gener-
 305 ally produces a fresh particle. When S_c , as calculated in equations (2)–(3), is
 306 used as the criterion for fresh versus aged, it can be shown that coagulation
 307 of two aged particles never produces a fresh particle, and that the coagulation
 308 of two fresh particles with S_c values close to the cutoff value can produce an
 309 aged particle.

Coagulation can result in a net loss of number but must conserve mass. We thus have

$$\dot{N}_a^{\text{coag}}(t) \leq \dot{N}_{f \rightarrow a}^{\text{coag}}(t) + \dot{N}_{a \rightarrow a}^{\text{coag}}(t) \quad (5)$$

$$\dot{M}_a^{\text{coag}}(t) = \dot{M}_{f \rightarrow a}^{\text{coag}}(t) + \dot{M}_{a \rightarrow a}^{\text{coag}}(t) \quad (6)$$

$$\Delta n_a^{\text{coag}}(t_{k-1}, t_k) \leq \Delta n_{f \rightarrow a}^{\text{coag}}(t_{k-1}, t_k) + \Delta n_{a \rightarrow a}^{\text{coag}}(t_{k-1}, t_k) \quad (7)$$

$$\Delta m_a^{\text{coag}}(t_{k-1}, t_k) = \Delta m_{f \rightarrow a}^{\text{coag}}(t_{k-1}, t_k) + \Delta m_{a \rightarrow a}^{\text{coag}}(t_{k-1}, t_k) \quad (8)$$

310 and similarly for coagulation resulting in fresh particles.

The following continuous equations describe the evolution of the number and

mass concentrations of fresh and aged BC-containing populations:

$$\begin{aligned} \frac{dN_f(t)}{dt} = & \dot{N}_f^{\text{density}}(t) + \dot{N}_f^{\text{emit}}(t) - \dot{N}_f^{\text{dilution}}(t) \\ & + \dot{N}_{a \rightarrow f}^{\text{cond}}(t) + \dot{N}_f^{\text{coag}}(t) - \dot{N}_{f \rightarrow f}^{\text{coag}}(t) - \underbrace{\left(\dot{N}_{f \rightarrow a}^{\text{cond}}(t) + \dot{N}_{f \rightarrow a}^{\text{coag}}(t) \right)}_{\dot{N}^{\text{aging}}(t)} \end{aligned} \quad (9)$$

$$\begin{aligned} \frac{dN_a(t)}{dt} = & \dot{N}_a^{\text{density}}(t) + \dot{N}_a^{\text{emit}}(t) - \dot{N}_a^{\text{dilution}}(t) \\ & + \dot{N}_{f \rightarrow a}^{\text{cond}}(t) + \dot{N}_a^{\text{coag}}(t) - \dot{N}_{a \rightarrow a}^{\text{coag}}(t) - \underbrace{\left(\dot{N}_{a \rightarrow f}^{\text{cond}}(t) + \dot{N}_{a \rightarrow f}^{\text{coag}}(t) \right)}_{\dot{N}^{\text{de-aging}}(t)} \end{aligned} \quad (10)$$

$$\begin{aligned} \frac{dM_f(t)}{dt} = & \dot{M}_f^{\text{density}}(t) + \dot{M}_f^{\text{emit}}(t) - \dot{M}_f^{\text{dilution}}(t) \\ & + \underbrace{\left(\dot{M}_{a \rightarrow f}^{\text{cond}}(t) + \dot{M}_{a \rightarrow f}^{\text{coag}}(t) \right)}_{\dot{M}^{\text{de-aging}}(t)} - \underbrace{\left(\dot{M}_{f \rightarrow a}^{\text{cond}}(t) + \dot{M}_{f \rightarrow a}^{\text{coag}}(t) \right)}_{\dot{M}^{\text{aging}}(t)} \end{aligned} \quad (11)$$

$$\begin{aligned} \frac{dM_a(t)}{dt} = & \dot{M}_a^{\text{density}}(t) + \dot{M}_a^{\text{emit}}(t) - \dot{M}_a^{\text{dilution}}(t) \\ & + \underbrace{\left(\dot{M}_{f \rightarrow a}^{\text{cond}}(t) + \dot{M}_{f \rightarrow a}^{\text{coag}}(t) \right)}_{\dot{M}^{\text{aging}}(t)} - \underbrace{\left(\dot{M}_{a \rightarrow f}^{\text{cond}}(t) + \dot{M}_{a \rightarrow f}^{\text{coag}}(t) \right)}_{\dot{M}^{\text{de-aging}}(t)} \end{aligned} \quad (12)$$

311 Note that the mass equations (11)–(12) have been simplified from forms identi-
 312 cal to the number equations (9)–(10) by using equation (6) for the conservation
 313 of mass during coagulation. Condensation (or rather evaporation) and coag-
 314 ulation can in principle also produce a transfer from aged to fresh particles.
 315 This is reflected by the terms denoted as $\dot{N}^{\text{de-aging}}(t)$ and $\dot{M}^{\text{de-aging}}(t)$ above.

The aging time-scales τ_N and τ_M for number and mass are then determined by the first-order models:

$$\dot{N}^{\text{aging}}(t) = \frac{1}{\tau_N(t)} N_f(t) \quad (13)$$

$$\dot{M}^{\text{aging}}(t) = \frac{1}{\tau_M(t)} M_f(t) \quad (14)$$

The discrete versions of the balance equations (9)–(12) are:

$$\begin{aligned} n_f(t_k) - n_f(t_{k-1}) = & \Delta n_f^{\text{emit}}(t_{k-1}, t_k) - \Delta n_f^{\text{dilution}}(t_{k-1}, t_k) \\ & + \Delta n_{a \rightarrow f}^{\text{cond}}(t_{k-1}, t_k) + \Delta n_f^{\text{coag}}(t_{k-1}, t_k) - \Delta n_{f \rightarrow f}^{\text{coag}}(t_{k-1}, t_k) \\ & - \underbrace{\left(\Delta n_{f \rightarrow a}^{\text{cond}}(t_{k-1}, t_k) + \Delta n_{f \rightarrow a}^{\text{coag}}(t_{k-1}, t_k) \right)}_{\Delta n^{\text{aging}}(t_{k-1}, t_k)} \end{aligned} \quad (15)$$

$$\begin{aligned}
n_a(t_k) - n_a(t_{k-1}) &= \Delta n_a^{\text{emit}}(t_{k-1}, t_k) - \Delta n_a^{\text{dilution}}(t_{k-1}, t_k) \\
&+ \Delta n_{f \rightarrow a}^{\text{cond}}(t_{k-1}, t_k) + \Delta n_a^{\text{coag}}(t_{k-1}, t_k) - \Delta n_{a \rightarrow a}^{\text{coag}}(t_{k-1}, t_k) \\
&- \underbrace{\left(\Delta n_{a \rightarrow f}^{\text{cond}}(t_{k-1}, t_k) + \Delta n_{a \rightarrow f}^{\text{coag}}(t_{k-1}, t_k) \right)}_{\Delta n^{\text{de-aging}}(t_{k-1}, t_k)}
\end{aligned} \tag{16}$$

$$\begin{aligned}
m_f(t_k) - m_f(t_{k-1}) &= \Delta m_f^{\text{emit}}(t_{k-1}, t_k) - \Delta m_f^{\text{dilution}}(t_{k-1}, t_k) \\
&+ \underbrace{\left(\Delta m_{a \rightarrow f}^{\text{cond}}(t_{k-1}, t_k) + \Delta m_{a \rightarrow f}^{\text{coag}}(t_{k-1}, t_k) \right)}_{\Delta m^{\text{de-aging}}(t_{k-1}, t_k)} \\
&- \underbrace{\left(\Delta m_{f \rightarrow a}^{\text{cond}}(t_{k-1}, t_k) + \Delta m_{f \rightarrow a}^{\text{coag}}(t_{k-1}, t_k) \right)}_{\Delta m^{\text{aging}}(t_{k-1}, t_k)}
\end{aligned} \tag{17}$$

$$\begin{aligned}
m_a(t_k) - m_a(t_{k-1}) &= \Delta m_a^{\text{emit}}(t_{k-1}, t_k) - \Delta m_a^{\text{dilution}}(t_{k-1}, t_k) \\
&+ \underbrace{\left(\Delta m_{f \rightarrow a}^{\text{cond}}(t_{k-1}, t_k) + \Delta m_{f \rightarrow a}^{\text{coag}}(t_{k-1}, t_k) \right)}_{\Delta m^{\text{aging}}(t_{k-1}, t_k)} \\
&- \underbrace{\left(\Delta m_{a \rightarrow f}^{\text{cond}}(t_{k-1}, t_k) + \Delta m_{a \rightarrow f}^{\text{coag}}(t_{k-1}, t_k) \right)}_{\Delta m^{\text{de-aging}}(t_{k-1}, t_k)}
\end{aligned} \tag{18}$$

316 Here equation (8) for the discrete conservation of mass during coagulation was
317 used to simplify the mass equations, as in the continuous case.

By comparing the continuous equations (9)–(12) to the discrete equations (15)–(18) using the relationships (4) we see that the continuous aging terms can be approximated by:

$$\dot{N}^{\text{aging}}(t_k) \approx \frac{\Delta n^{\text{aging}}(t_{k-1}, t_k)}{(t_k - t_{k-1})V(t_k)} \tag{19}$$

$$\dot{M}^{\text{aging}}(t_k) \approx \frac{\Delta m^{\text{aging}}(t_{k-1}, t_k)}{(t_k - t_{k-1})V(t_k)}, \tag{20}$$

318 where the use of V at time t_k is because the computational volume V is
319 updated first within each timestep in the PartMC algorithm (Riemer et al.,
320 2009, Figure 1).

From equations (13) and (14) and the relationships (4), the aging time-scales τ_N and τ_M are then approximated by:

$$\tau_N(t_k) \approx \frac{(t_k - t_{k-1})n_f(t_k)}{\Delta n^{\text{aging}}(t_{k-1}, t_k)} \tag{21}$$

$$\tau_M(t_k) \approx \frac{(t_k - t_{k-1})m_f(t_k)}{\Delta m^{\text{aging}}(t_{k-1}, t_k)}. \tag{22}$$

For the analysis in Section 5 we additionally define the aging time-scale τ_N^{cond} ignoring the impact of coagulation, an average time-scale $\tau_{N,\text{day}}$ during the day, and an average time-scale $\tau_{N,\text{night}}$ during the night, given by:

$$\tau_N^{\text{cond}}(t_k) \approx \frac{(t_k - t_{k-1})n_f(t_k)}{\Delta n_{f \rightarrow a}^{\text{cond}}(t_{k-1}, t_k)} \quad (23)$$

$$(\tau_{N,\text{day}})^{-1} = \frac{1}{3 \text{ hours}} \int_{12:00 \text{ LST}}^{15:00 \text{ LST}} (\tau_N(t))^{-1} dt \quad (24)$$

$$(\tau_{N,\text{night}})^{-1} = \frac{1}{10 \text{ hours}} \int_{18:00 \text{ LST}}^{04:00 \text{ LST}} (\tau_N(t))^{-1} dt, \quad (25)$$

321 and similarly for τ_M^{cond} , $\tau_{M,\text{day}}$, $\tau_{M,\text{night}}$, $\tau_{N,\text{day}}^{\text{cond}}$, and so on.

322 5 Results

323 In this section we show results for supersaturation thresholds ranging between
 324 $S_c = 0.1\%$ and $S_c = 1.0\%$, as these are typically achieved in updrafts in
 325 stratus and cumulus clouds (Warner, 1968). To limit the number of figures we
 326 use $S_c = 0.6\%$ as a base case. Figure 5 shows the time series for N_f , N_a , and
 327 $N_{\text{BC}} = N_f + N_a$ for $S_c = 0.6\%$. The total number concentration N_{BC} of BC-
 328 containing particles increased until 18:00 LST due to the emission of particles.
 329 After the emissions stopped, N_{BC} decreased as a result of continued dilution
 330 and coagulation. The time series for N_f and N_a show that both increased
 331 in the morning hours. A pronounced transfer from fresh to aged occurred
 332 after 11:30 LST, the time when nitrate formation started taking place on the
 333 dry particles (compare Figure 2). This process efficiently contributed to the
 334 conversion of fresh particles to aged particles, which was reflected by a short
 335 aging time-scale.

336 The left column of Figure 6 compares the aging time-scales τ_N and τ_N^{cond}
 337 computed according to equations (21) and (23) for different supersaturation
 338 thresholds. The top, middle and bottom panels shows the results for super-
 339 saturation thresholds $S_c = 0.1\%$, $S_c = 0.6\%$, and $S_c = 1\%$, respectively. The
 340 grey shading is the raw data, and the black lines are results computed from
 341 smoothing the transfer rates with a Hann filter with a window width of 1 hour.

342 The solid lines represent τ_N , including the contributions due to both coagula-
 343 tion and condensation according to equation (21). For $S_c = 0.6\%$, τ_N started
 344 off in the morning with values of $\tau_N \approx 20$ hours. It decreased sharply after
 345 11:00 LST, which is the time when photochemistry was at its peak, and ni-
 346 trate formation was most pronounced, hence leading to a fast aging process.
 347 Between 12:00 LST and 16:00 LST, τ_N was less than 1 hour, and reached val-
 348 ues as low as 0.2 hours. After 16:00 LST, as photochemistry slowed down, τ_N

349 increased again, reaching a plateau of $\tau_N \approx 10$ hours during the evening and
350 night.

351 The broken lines represent τ_N^{cond} as defined in equation (23), i.e. the contribu-
352 tion due to coagulation is ignored. There was only a small difference between τ_N
353 and τ_N^{cond} during midday and early afternoon when condensation was operat-
354 ing very effectively. However during morning, afternoon and night, neglecting
355 coagulation lead to larger time-scales (up to one order of magnitude).

356 A similar pattern was found for $S_c = 1\%$, shown in the bottom panel. For
357 $S_c = 0.1\%$ we generally obtained larger time-scales. During the morning, τ_N
358 was about 50 hours and decreased to 10 hours in the early afternoon. There
359 was a short period around 16:00 LST when τ_N dropped to 2 hours. Obviously,
360 at $S_c = 0.1\%$, even after the growth due to condensation of ammonium nitrate,
361 the particles were still too small to be activated to the same extent as seen
362 for the larger supersaturations. During the following night τ_N was around 10–
363 20 hours. For this low supersaturation the contrast between day and night was
364 not as pronounced as for $S_c = 0.6\%$ or $S_c = 1\%$.

365 Qualitatively, the temporal evolution of τ_M (right column) was similar to the
366 number-based result τ_N . However the day/night contrast was more pronounced
367 for the case with $S_c = 0.1\%$, and the time-scales based on mass during the
368 day were lower than the ones based on number.

369 Figure 7 shows the individual transfer terms of BC-containing particles for the
370 case $S_c = 0.6\%$. The transfer rate $\dot{N}_{a \rightarrow f}^{\text{coag}}$ due to coagulation from aged to fresh
371 was very small throughout the whole day, remaining below $0.01 \text{ cm}^{-3} \text{ s}^{-1}$. The
372 transfer rate $\dot{N}_{f \rightarrow a}^{\text{coag}}$ due to coagulation from fresh to aged followed the time
373 series of N_f . The minimum of N_f during the early afternoon was reflected in
374 a minimum of the transfer rate $\dot{N}_{f \rightarrow a}^{\text{coag}}$. The transfer rate $\dot{N}_{f \rightarrow a}^{\text{cond}}$ due to conden-
375 sation from fresh to aged was large between 11:30 and 15:00 LST, consistent
376 with the decrease of τ_N in Figure 6. Lastly, there was a non-zero transfer $\dot{N}_{a \rightarrow f}^{\text{cond}}$
377 from aged to fresh due to condensation, which was larger than $\dot{N}_{f \rightarrow a}^{\text{cond}}$ towards
378 the end of the simulation. This was related to a shrinking of the particles due
379 to decreasing relative humidity (compare Figure 1).

380 Figure 8 summarizes the results for the different aging time-scale definitions.
381 We calculated $\tau_{N,\text{day}}$ and $\tau_{N,\text{night}}$ according to equation (23) for several hundred
382 different supersaturation thresholds between $S_c = 0.1\%$ and $S_c = 1\%$. We
383 also distinguished between the definition of τ including the transfer due to
384 coagulation and condensation (solid lines), and including only the transfer
385 due to condensation, $\tau_{N,\text{day}}^{\text{cond}}$ and $\tau_{N,\text{night}}^{\text{cond}}$ (broken lines).

386 For this particular urban plume scenario the following general features emerge:
387 during the day, condensation of semi-volatile species, in our case especially am-
388 monium nitrate, was the dominant process for aging. The time-scales based

389 on number were larger than the time-scales based on mass during the day,
390 by roughly a factor of five. The aging time-scales had a strong dependence
391 on supersaturation threshold. For $S_c = 0.1\%$, $\tau_{N,\text{day}}$ was 10 hours, whereas for
392 $S_c = 1\%$, $\tau_{N,\text{day}}$ was only 0.2 hours. During the night condensation was limited,
393 hence coagulation was the dominant aging process. For low supersaturation
394 thresholds, the time-scales based on number were smaller than the time-scales
395 based on mass, but this difference decreased for higher supersaturation thresh-
396 olds.

397 6 Conclusions

398 In this paper we presented a method for explicitly calculating aging time-
399 scales of black carbon aerosol using particle-resolved model simulations with
400 PartMC-MOSAIC. We developed number-based and mass-based aging time-
401 scales using the activation of the particles at a given supersaturation as a cri-
402 terion for aging. We applied this method to an urban plume scenario (Riemer
403 et al., 2009) for a range of supersaturation thresholds between 0.1% and 1%
404 and considered condensation of secondary substances and coagulation as aging
405 mechanisms. Aging due to heterogeneous processes (chemical aging) were not
406 included.

407 For this particular scenario we found a separation into day and night regimes.
408 During the day the condensation-induced aging dominated, in particular due
409 to the formation of ammonium nitrate. Therefore the condensation-only number-
410 based aging time-scale $\tau_{N,\text{day}}^{\text{cond}}$ was almost the same as the total time-scale $\tau_{N,\text{day}}$
411 and similarly for mass. The daytime aging number-based time-scale $\tau_{N,\text{day}}$ was
412 about 10 hours for a supersaturation threshold of $S_c = 0.1\%$ and decreased to
413 0.06 hours for a threshold of $S_c = 1\%$. The daytime mass-based aging time-
414 scale $\tau_{M,\text{day}}$ was about a factor of five lower than $\tau_{N,\text{day}}$ for all supersaturation
415 thresholds.

416 During the night, the absence of condensable species caused the number-based
417 aging time-scale $\tau_{N,\text{night}}$ to be about one order of magnitude larger than during
418 the day. Coagulation became dominant, which was reflected by the fact that
419 the condensation-only time-scale $\tau_{N,\text{night}}^{\text{cond}}$ was an order of magnitude larger
420 than the total time-scale $\tau_{N,\text{night}}$. The nighttime aging time-scales therefore
421 depended on the particle number concentrations. We suspect that chemical
422 aging would have its largest impact during periods when condensation is not
423 dominant, i.e. during the night in our case.

424 Compared to the time-scales used in global models, which are typically on the
425 order of 30 hours (Chung and Seinfeld, 2002; Koch, 2001, e.g.), our time-scales
426 were much shorter, in particular during the day. This confirmed findings by

427 Riemer et al. (2004) who showed with a completely different approach that
428 daytime and nighttime aging regimes exists, and that aging during the day
429 proceeds very rapidly.

430 However some caveats need to be emphasized: our urban plume scenario repre-
431 sents only one scenario, with very polluted conditions and fairly high number
432 concentrations during the night ($N_{BC} \approx 5000 \text{ cm}^{-3}$). For lower number con-
433 centrations, we expect the aging time-scales during the night to increase.

434 **Acknowledgments.** Funding for N. Riemer and M. West was provided by
435 the National Science Foundation (NSF) under grant ATM 0739404. Funding
436 for R. A. Zaveri and R. C. Easter was provided by the Aerosol-Climate Initia-
437 tive as part of the Pacific Northwest National Laboratory (PNNL) Laboratory
438 Directed Research and Development (LDRD) program. Pacific Northwest Na-
439 tional Laboratory is operated for the U.S. Department of Energy by Battelle
440 Memorial Institute under contract DE-AC06-76RLO 1830.

441 References

- 442 Andreae, M., Gelencsér, A., 2006. Black carbon or brown carbon? The nature
443 of light-absorbing carbonaceous aerosols. *Atmos. Chem. Phys.* 6, 3131–3148.
- 444 Bond, T., Streets, D., Yarber, K., Nelson, S., Woo, J., Klimont, Z., 2004. A
445 technology-based global inventory of black and organic carbon emissions
446 from combustion. *J. Geophys. Res.* 109 (D14), D14203.
- 447 Chung, S. H., Seinfeld, J. H., 2002. Global distribution and climate forcing of
448 carbonaceous aerosols. *J. Geophys. Res.* 107.
- 449 Clegg, S., Brimblecombe, P., Wexler, A., 1998. Thermodynamic model of the
450 system $\text{H}^+\text{-NH}_4^+\text{-Na}^+\text{-SO}_4^{2-}\text{-NH}_3\text{-Cl}^-\text{-H}_2\text{O}$ at 298.15 K. *J. Phys. Chem. A*
451 102 (12), 2155–2171.
- 452 Cooke, W. F., Lioussé, C., Cachier, H., Feichter, J., 1999. Construction of a
453 $1^\circ \times 1^\circ$ fossil fuel emission data set for carbonaceous aerosol and implemen-
454 tation and radiative impact in the ECHAM4 model. *J. Geophys. Res.* 104,
455 22137–22162.
- 456 Croft, B., Lohmann, U., von Salzen, K., 2005. Black carbon aging in the
457 Canadian Centre for Climate modelling and analysis atmospheric general
458 circulation model. *Atmos. Chem. Phys.* 5, 1931–1949, sRef-ID:1680-
459 7324/acp/2005-5-1931.
- 460 Cubison, M. J., Ervens, B., Feingold, G., Docherty, K. S., Ulbrich, I. M.,
461 Shields, L., Prather, K., Hering, S., Jimenez, J. L., 2008. The influence of
462 chemical composition and mixing state on Los Angeles urban aerosol on
463 CCN number and cloud properties. *Atmos. Chem. Phys. Discuss.* 8, 5629–
464 5681.

- 465 Eldering, A., Cass, G. R., 1996. Source-oriented model for air pollution effects
466 on visibility. *J. Geophys. Res.* 101, 19343–19369.
- 467 Furutani, H., Dallosto, M., Roberts, G., Prather, K., 2008. Assessment of the
468 relative importance of atmospheric aging on CCN activity derived from field
469 observations. *Atmos. Environ.* 42 (13), 3130–3142.
- 470 Ghan, S., Laulainen, N., Easter, R., Wagener, R., Nemesure, S., Chapman, E.,
471 Zhang, Y., Leung, R., 2001. Evaluation of aerosol direct radiative forcing in
472 MIRAGE. *Journal of Geophysical Research* 106 (D6), 5317–5334.
- 473 Horvath, H., Trier, A., 1993. A study of the aerosol of Santiago de Chile — I.
474 Light extinction coefficient. *Atmos. Environ.* 27, 371–384.
- 475 IPCC, 2007. *Climate Change 2007: The physical science basis summary for*
476 *policymakers. Contribution of working group I to the fourth assessment re-*
477 *port of the Intergovernmental Panel on Climate Change.* World Meteorolo-
478 *gical Organization, Geneva, Switzerland.*
- 479 Jaenicke, R., 1993. *Aerosol-Cloud-Climate Interaction.* Academic Press, San
480 *Diego, CA, Ch. Tropospheric aerosols, pp. 1–31.*
- 481 Kittelson, D., Watts, W., Johnson, J., 2006a. On-road and laboratory evalu-
482 ation of combustion aerosols — Part 1: Summary of diesel engine results.
483 *Aerosol Sci.* 37, 913–930.
- 484 Kittelson, D., Watts, W., Johnson, J., Schauer, J., Lawson, D., 2006b. On-
485 road and laboratory evaluation of combustion aerosols — Part 2: Summary
486 of spark ignition engine results. *Aerosol Sci.* 37, 931–949.
- 487 Kleeman, M., Schauer, J., Cass, G., 2000. Size and composition distribution of
488 fine particulate matter emitted from motor vehicles. *Environ. Sci. Technol.*
489 34, 1132–1142.
- 490 Koch, D., 2001. Transport and direct radiative forcing of carbonaceous and
491 sulfate aerosols in the GISS GCM. *J. Geophys. Res.* 106, 20311–20332.
- 492 Lohmann, U., Feichter, J., Chuang, C. C., Penner, J. E., 1999. Prediction of
493 the number of cloud droplets in the ECHAM GCM. *J. Geophys. Res.* 104,
494 9169–9198.
- 495 McFiggans, G., Artaxo, P., Baltensperger, U., Coe, H., Facchini, M. C., Fein-
496 gold, G., Fuzzi, S., Gysel, M., Laaksonen, A., Lohmann, U., Mentel, T. F.,
497 Murphy, D. M., O’Dowd, C. D., Snider, J. R., Weingartner, E., 2006. The
498 effect of physical and chemical aerosol properties on warm cloud droplet
499 activation. *Atmos. Chem. Phys.* 6, 2593–2649.
- 500 McMurry, P., Stolzenburg, M., 1989. On the sensitivity of particle size to
501 relative humidity for Los Angeles aerosols. *Atmospheric Environment* (1967)
502 23 (2), 497–507.
- 503 Medalia, A., Rivin, D., 1982. Particulate carbon and other components of soot
504 and carbon black. *Carbon* 20, 481–492.
- 505 Menon, S., Hansen, J., Nazarenko, L., Luo, Y. F., 2002. Climate effects of
506 black carbon aerosols in China and India. *Science* 297, 2250–2253.
- 507 Moffet, R., Qin, X., Rebotier, T., Furutani, H., Prather, K., 2008. Chemically
508 segregated optical and microphysical properties of ambient aerosols mea-
509 sured in a single-particle mass spectrometer. *J. Geophys. Res.* 113 (D12),

510 D12213.

511 Petters, M., Prenni, A., Kreidenweis, S., DeMott, P., Matsunaga, A., Lim,
512 Y., Ziemann, P., 2006. Chemical aging and the hydrophobic-to-hydrophilic
513 conversion of carbonaceous aerosol. *Geophys. Res. Lett* 33, L24806.

514 Petters, M. D., Kreidenweis, S. M., 2007. A single parameter representation of
515 hygroscopic growth and cloud condensation nucleus activity. *Atmos. Chem.*
516 *Phys.* 7, 1961–1971.

517 Pöschl, U., 2005. Atmospheric aerosols: Composition, transformation, climate
518 and health effects. *Angew. Chem. Int. Ed. Engl.* 44, 752–754.

519 Prenni, A., Petters, M., Kreidenweis, S., DeMott, P., Ziemann, P., 2007.
520 Cloud droplet activation of secondary organic aerosol. *J. Geophys. Res* 112,
521 D10223.

522 Press, W. H., Teukolsky, S. A., Vetterling, W. T., Flannery, B. P., 2007. *Nu-*
523 *merical Recipes: The Art of Scientific Computing*, 3rd Edition. Cambridge
524 University Press.

525 Riemer, N., Vogel, H., Vogel, B., 2004. Soot aging time scales in polluted
526 regions during day and night. *Atmospheric Chemistry and Physics* 4, 1885–
527 1893.

528 Riemer, N., Vogel, H., Vogel, B., Fiedler, F., 2003. Modeling aerosols on the
529 mesoscale γ , part I: Treatment of soot aerosol and its radiative effects. *J.*
530 *Geophys. Res.* 108, 4601.

531 Riemer, N., West, M., Zaveri, R., Easter, R., 2009. Simulating the evolution of
532 soot mixing state with a particle-resolved aerosol model. *J. Geophys. Res.*In
533 press.

534 Rudich, Y., Donahue, N. M., Mentel, T. F., 2007. Aging of organic aerosol:
535 Bridging the gap between laboratory and field studies. *Annual Rev. Phys.*
536 *Chem.* 58, 321–352.

537 Schell, B., Ackermann, I. J., Binkowski, F. S., Ebel, A., 2001. Modeling the
538 formation of secondary organic aerosol within a comprehensive air quality
539 model system. *J. Geophys. Res.* 106, 28275–28293.

540 Svenningsson, B., Rissler, J., Swietlicki, E., Mircea, M., Bilde, M., Facchini,
541 M., Decesari, S., Fuzzi, S., Zhou, J., Mønster, J., et al., 2006. Hygroscopic
542 growth and critical supersaturations for mixed aerosol particles of inorganic
543 and organic compounds of atmospheric relevance. *Atmos. Chem. Phys* 6,
544 1937–1952.

545 Toner, S., Sodeman, S., Prather, K., 2006. Single particle characterization of
546 ultrafine and accumulation mode particles from heavy duty diesel vehicles
547 using aerosol time-of-flight mass spectrometry. *Environ. Sci. Technol.* 40,
548 3912–3921.

549 Warner, J., 1968. The supersaturation in natural clouds. *J. Appl. Meteorol.*
550 7, 233–237.

551 Weingartner, E., Burtscher, H., Baltensperger, H., 1997. Hygroscopic proper-
552 ties of carbon and diesel soot particles. *Atmos. Environ.* 31, 2311–2327.

553 Zaveri, R. A., Easter, R. C., Fast, J. D., Peters, L. K., 2008. Model for Sim-
554 ulating Aerosol Interactions and Chemistry (MOSAIC). *J. Geophys. Res.*

555 113, D13204.
556 Zaveri, R. A., Easter, R. C., Peters, L. K., 2005a. A computationally efficient
557 Multicomponent Equilibrium Solver for Aerosols (MESA). *J. Geophys. Res.*
558 110, D24203.
559 Zaveri, R. A., Easter, R. C., Wexler, A. S., 2005b. A new method for multicom-
560 ponent activity coefficients of electrolytes in aqueous atmospheric aerosols.
561 *J. Geophys. Res.* 110, D02210, doi:10.1029/2004JD004681.
562 Zaveri, R. A., Peters, L. K., 1999. A new lumped structure photochemical
563 mechanism for large-scale applications. *J. Geophys. Res.* 104, 30387–30415.

Initial/Background	N (m^{-3})	D_{gn} (μm)	σ_{g} (1)	Composition by mass
Aitken Mode	$3.2 \cdot 10^9$	0.02	1.45	50% $(\text{NH}_4)_2\text{SO}_4$, 50% POA
Accumulation Mode	$2.9 \cdot 10^9$	0.116	1.65	50% $(\text{NH}_4)_2\text{SO}_4$, 50% POA

Emissions	E ($\text{m}^{-2} \text{s}^{-1}$)	D_{gn} (μm)	σ_{g} (1)	Composition by mass
Meat cooking	$9 \cdot 10^6$	0.086	1.9	100% POA
Diesel vehicles	$1.6 \cdot 10^8$	0.05	1.7	30% POA, 70% BC
Gasoline vehicles	$5 \cdot 10^7$	0.05	1.7	80% POA, 20% BC

Table 1

Initial and emitted aerosol distribution parameters. The initial aerosol distribution is also used as the background aerosol distribution. The percentages for the composition are by mass. E is the area source strength of particle emissions. Dividing E by the mixing height and multiplying by a normalized composition distribution gives the number distribution emission rate.

Terms	Description
$N_f(t), N_a(t)$	Number concentration of fresh/aged BC-containing particles.
$\dot{N}_f^{\text{emit}}(t), \dot{N}_a^{\text{emit}}(t)$	Gain rate of number concentration of fresh/aged BC-containing particles due to emission.
$\dot{N}_f^{\text{dilution}}(t), \dot{N}_a^{\text{dilution}}(t)$	Loss rate of number concentration of fresh/aged BC-containing particles due to dilution.
$\dot{N}_{f \rightarrow a}^{\text{cond}}(t), \dot{N}_{a \rightarrow f}^{\text{cond}}(t)$	Gain rate of number concentration of aged/fresh BC-containing particles due to condensation or evaporation on fresh/aged particles.
$\dot{N}_f^{\text{coag}}(t), \dot{N}_a^{\text{coag}}(t)$	Gain rate of number concentration of fresh/aged BC-containing particles from coagulation events.
$\dot{N}_{f \rightarrow f}^{\text{coag}}(t), \dot{N}_{f \rightarrow a}^{\text{coag}}(t)$	Loss rate of number concentration of fresh BC-containing particles to coagulation events resulting in fresh/aged particles.
$\dot{N}_{a \rightarrow a}^{\text{coag}}(t), \dot{N}_{a \rightarrow f}^{\text{coag}}(t)$	Loss rate of number concentration of aged BC-containing particles to coagulation events resulting in aged/fresh particles.
$\dot{N}_f^{\text{density}}(t), \dot{N}_a^{\text{density}}(t)$	Gain rate of number concentration of fresh/aged BC-containing particles due to air density changes.
$\dot{N}^{\text{aging}}(t), \dot{N}^{\text{de-aging}}(t)$	Net transfer rate of fresh-to-aged/aged-to-fresh number concentration of BC-containing particles.

Table 2

Description of individual terms in equations (9) and (10). With the exception of $\dot{N}_f^{\text{density}}(t)$ and $\dot{N}_a^{\text{density}}(t)$ all of these terms must be non-negative. The same notation is for the terms in equations (11) and (12) for mass concentration, and for the corresponding discrete equations (15)–(18). The discrete terms are expressed as a change in number or mass within a timestep, so that $\Delta n_{f \rightarrow a}^{\text{cond}}(t_{k-1}, t_k)$ is the number of BC-containing particles in the computational volume that change from fresh to aged due only to condensation during the timestep from time t_{k-1} to t_k , for example. There are no discrete terms for air density changes as they are incorporated by changing the computational volume V .

Particle 1	Particle 2	Resulting particle	Non-zero loss terms	Non-zero gain terms
fresh	fresh	fresh	$\Delta n_{f \rightarrow f}^{\text{coag}} = 2$	$\Delta n_f^{\text{coag}} = 1$
fresh	fresh	aged	$\Delta n_{f \rightarrow a}^{\text{coag}} = 2$	$\Delta n_a^{\text{coag}} = 1$
aged	fresh	fresh	$\Delta n_{a \rightarrow f}^{\text{coag}} = 1, \Delta n_{f \rightarrow f}^{\text{coag}} = 1$	$\Delta n_f^{\text{coag}} = 1$
aged	fresh	aged	$\Delta n_{a \rightarrow a}^{\text{coag}} = 1, \Delta n_{f \rightarrow a}^{\text{coag}} = 1$	$\Delta n_a^{\text{coag}} = 1$
aged	aged	aged	$\Delta n_{a \rightarrow a}^{\text{coag}} = 2$	$\Delta n_a^{\text{coag}} = 1$
fresh	non-BC	fresh	$\Delta n_{f \rightarrow f}^{\text{coag}} = 1$	$\Delta n_f^{\text{coag}} = 1$
fresh	non-BC	aged	$\Delta n_{f \rightarrow a}^{\text{coag}} = 1$	$\Delta n_a^{\text{coag}} = 1$
aged	non-BC	fresh	$\Delta n_{a \rightarrow f}^{\text{coag}} = 1$	$\Delta n_f^{\text{coag}} = 1$
aged	non-BC	aged	$\Delta n_{a \rightarrow a}^{\text{coag}} = 1$	$\Delta n_a^{\text{coag}} = 1$

Table 3

The different coagulation events and the resulting expressions for the loss and gain terms of the number of fresh and aged BC-containing particles. Similar expressions exist for mass changes Δm in the particle-resolved model and for the number rates \dot{N} and mass rates \dot{M} in the continuous model.

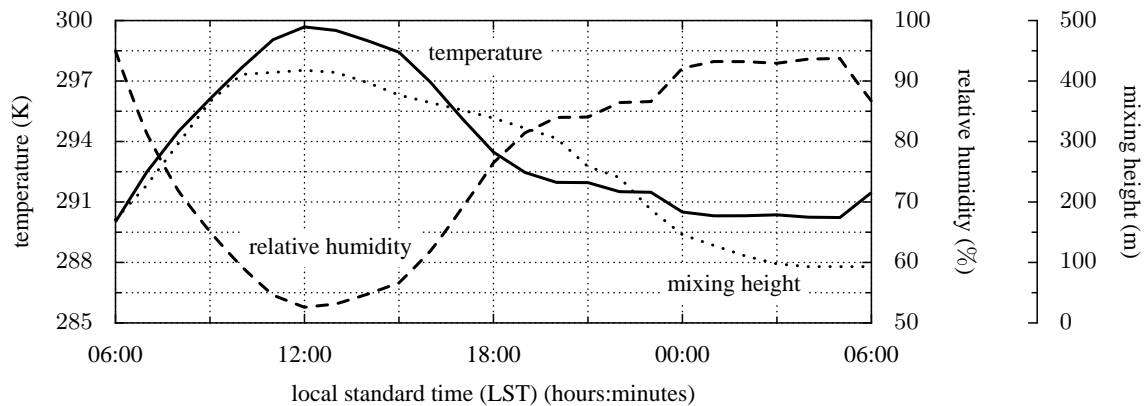


Fig. 1. Time series of temperature, relative humidity, and mixing height over the course of the 24 hour simulation. The pressure and water mixing ratio were kept constant.

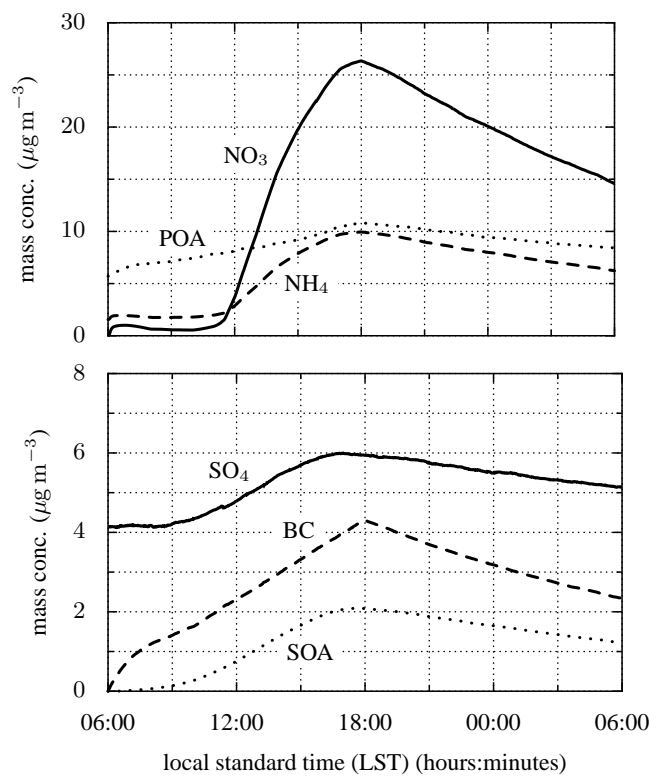


Fig. 2. Time series of mass concentrations of selected aerosol species: nitrate (NO_3), ammonium (NH_4), POA, sulfate (SO_4), BC, and SOA. Particle and gas phase emissions were present from 06:00 to 18:00 LST.

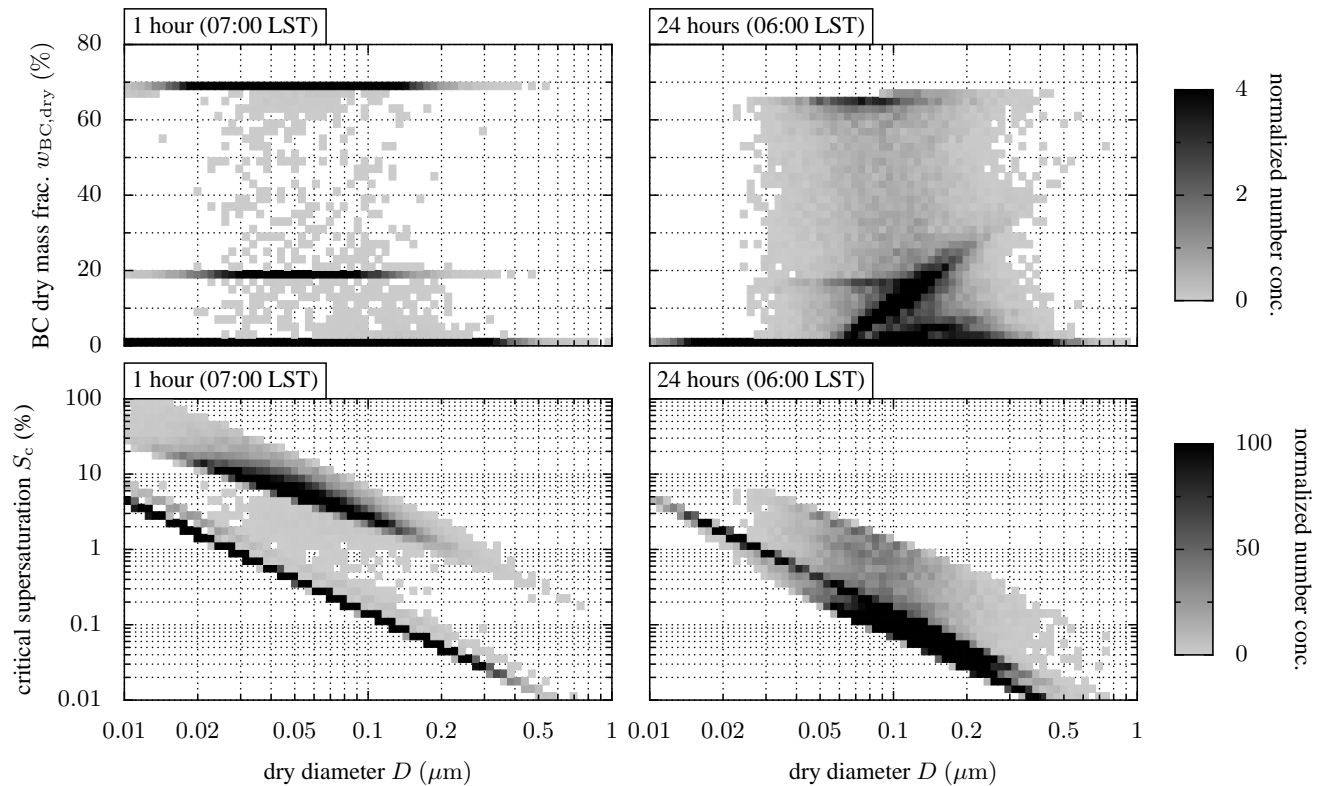


Fig. 3. Normalized two-dimensional number distributions after 1 hour (07:00 LST) and 24 hours (06:00 LST the next day) of simulation. The top panels show the normalized value of the two-dimensional distribution $\partial^2 N_{\text{BC,dry}}(D, w)/(\partial \log_{10} D \partial w)$ with respect to diameter D and BC dry mass fraction $w_{\text{BC,dry}}$, while the bottom panels show the normalized value of the two-dimensional distribution $\partial^2 N_{\text{S}}(D, S_c)/(\partial \log_{10} D \partial \log_{10} S_c)$ with respect to diameter D and critical supersaturation S_c .

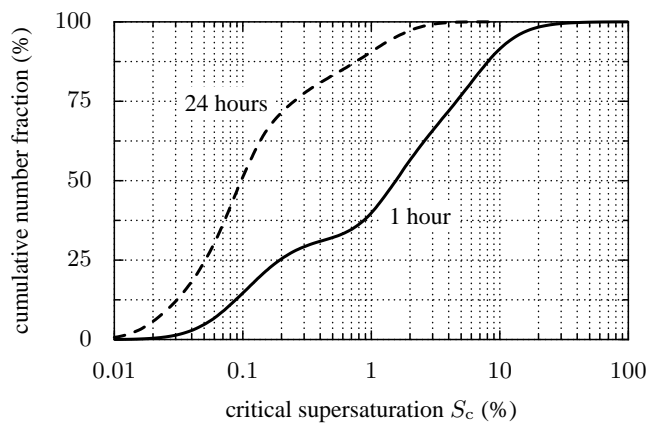


Fig. 4. Cloud condensation nuclei spectra after 1 hour (07:00 LST) and 24 hours (06:00 LST the next day) of simulation based on the simulation results shown in Figure 3.

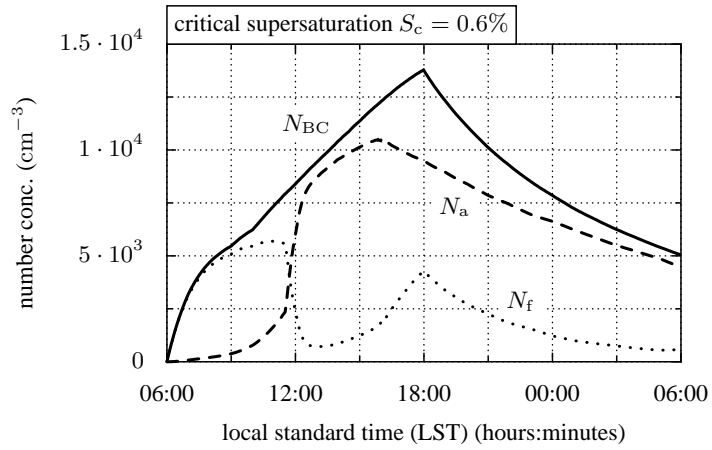


Fig. 5. Time series of total number concentration N_{BC} of BC-containing particles and number concentrations N_{f} and N_{a} for fresh and aged BC-containing particles, respectively. The critical supersaturation separating fresh and aged particles is set to $S_{\text{c}} = 0.6\%$.

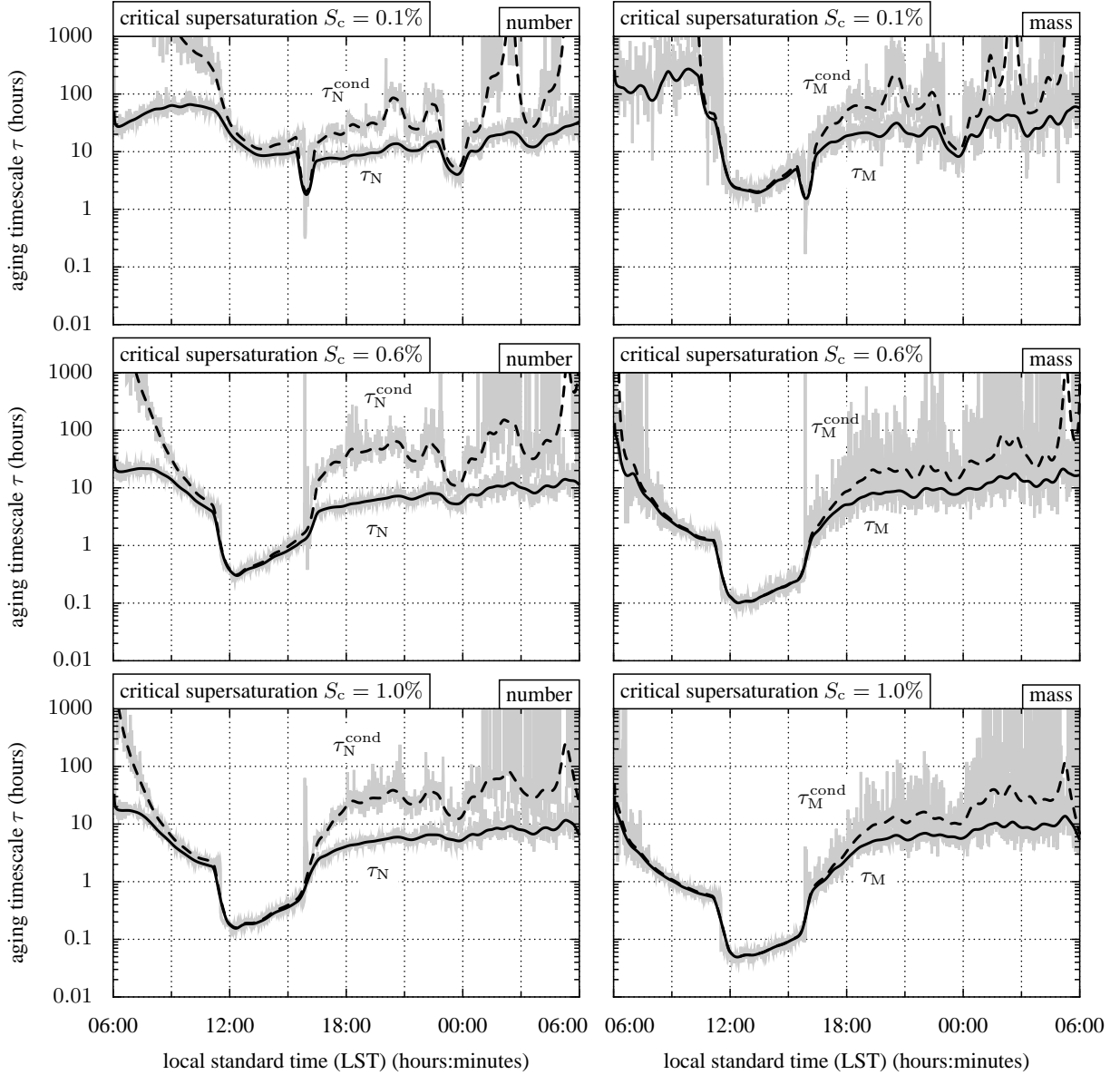


Fig. 6. Comparison of aging time-scales based on number (left) and mass (right), showing both the time-scales due to condensation and coagulation (τ_N and τ_M) and the time-scales due to condensation alone (τ_N^{cond} and τ_M^{cond}). The top panels have the critical supersaturation separating fresh from aged particles set to $S_c = 0.1\%$, while the middle panels have $S_c = 0.6\%$, and the bottom panels have $S_c = 1.0\%$.

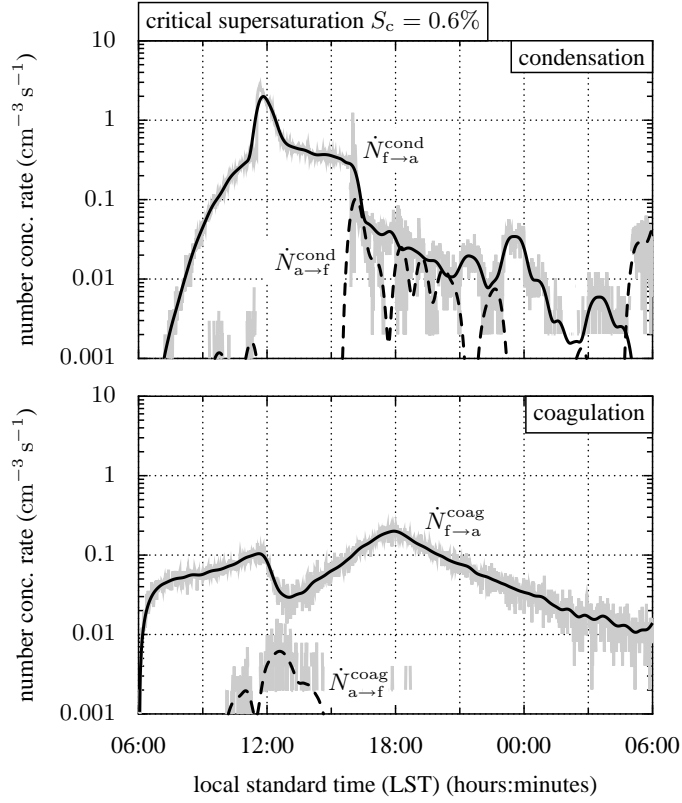


Fig. 7. Transfer rates due to condensation (top) and coagulation (bottom). The critical supersaturation separating fresh and aged particles is set to $S_c = 0.6\%$. The notation is according to Table 2.

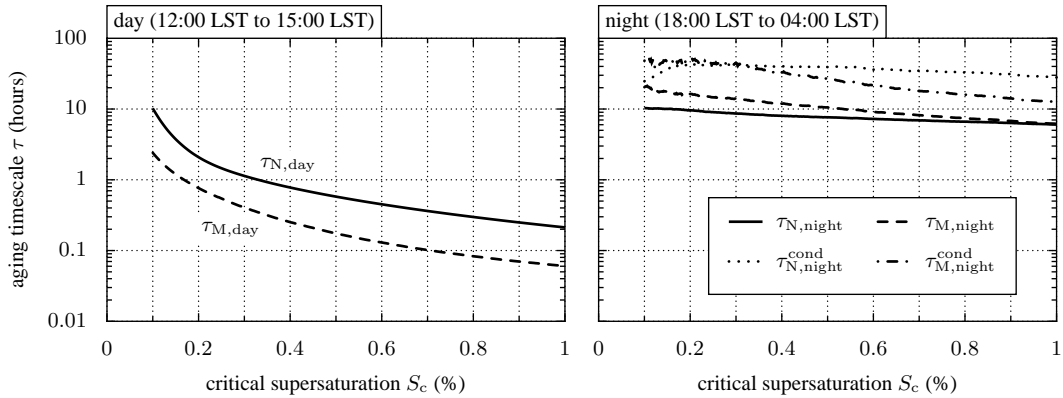


Fig. 8. Day (left) and night (right) averages of the aging time-scale, as defined in equations (23)–(25). As can be seen from Figure 6, during the day the condensation-induced aging dominates, so $\tau_{N,\text{day}}^{\text{cond}}$ is almost indistinguishable from $\tau_{N,\text{day}}$, and similarly for mass.